fiber chromatic dispersion. However, the phase noise from the beating of signal with noise also spreads to adjacent pulse, causing IXPM-induced nonlinear phase noise. The combined nonlinear phase noise of dispersive transmission system is larger than the impact of IFWM-induced ghost pulses.

1. Pulse Overlap in Dispersive Fiber

Fiber dispersion broadens the optical pulses and limits the transmission distance of an optical signal. Chromatic dispersion was studied in Sec. 4.4 based on computer simulation. While the impact of chromatic dispersion to practical signal must be studied using computer simulation, analytical results are available for Gaussian pulse in a dispersive fiber.

For simplicity, assume that the pulse launched into the optical fiber has a low pass representation of

$$u_0(0,t) = A_0 \exp\left[-\frac{1}{2}\left(\frac{t}{T_0}\right)^2\right], \tag{7.1}$$

as a Gaussian pulse with a peak amplitude of A_0, where T_0 is the $1/e$ width of the pulse intensity, and $1.66T_0$ is full-width-half-maximum (FWHM) pulse width. Based on the simple model of Eq. (4.46) in Sec. 4.4, the pulse spectrum at the distance of z is

$$B(z,\omega) = A_0\sqrt{2\pi}T_0 \exp\left[-\frac{\omega^2 T_0^2 - j\beta_2\omega^2}{2}\right], \tag{7.2}$$

with a pulse shape of

$$u_0(z,t) = \frac{A_0 T_0}{(T_0^2 - j\beta_2 z)^{1/2}} \exp\left[-\frac{t^2}{2(T_0^2 - j\beta_2 z)}\right], \tag{7.3}$$

where β_2 is the group velocity dispersion coefficient. After a distance of z, the pulse of Eq. (7.1) broadens to an $1/e$ pulse width of

$$\tau(z) = \sqrt{T_0^2 + \beta_2^2 z^2/T_0^2}. \tag{7.4}$$

A Gaussian pulse is broadened with distance from Eq. (7.4), for short pulse with small initial pulse width of T_0, the pulse width increases linearly with distance as $\tau(z) \approx |\beta_2|z/T_0$. For 40-Gb/s system with $T = 25$ ps and using RZ pulses with duty-cycle of 50% of $T_0 = 7.53$ ps. In typical standard single-mode fiber, $\beta_2 = -21.7$ ps^2/km, corresponding to $D = 17$ ps/km/nm at the wavelength of 1.55 μm. The pulse width

is doubled just after a short distance of about 4.5 km, far shorter than the effective nonlinear length of $L_{\text{eff}} \approx 1/\alpha = 21.7$ km. When $z = L_{\text{eff}}$, the pulse width is already $8.5T_0$ in this particular case. For low-power linear transmission, dispersion compensation can be used at the end of the fiber to return the original launched pulse. When optical amplifiers are used periodically to boost up the power, nonlinear pulse-to-pulse interaction is very strong in the system due to pulse overlap.

Pulse overlap is reduced for system with small fiber dispersion. For example, if fiber dispersion coefficient is $D = 3.5$ ps/km/nm, typically for nonzero dispersion-shifted fiber (NZDSF), the pulse width is doubled after a fiber distance of 22.3 km. For low speed system with long pulse width, for example, 10-Gb/s system with $T_0 = 30.1$ ps, the pulse width is doubled after a fiber distance of 71.4 km for $D = 17$ ps/km/nm. Pulse-to-pulse interaction is a particular problem mostly for 40 Gb/s systems, especially for system using standard single-mode fiber with large dispersion.

The above analysis for Gaussian pulse is largely based on Marcuse (1980, 1981), and Agrawal (2002). We assume a zero-chirp Gaussian pulse for simplicity. Both Marcuse (1981) and Agrawal (2002) derive the pulse broadening for chirp Gaussian pulse. For non-Gaussian pulses or fiber with large third-order dispersion, there is no analytical solution for the pulse shape but the pulse width (Marcuse, 1980, 1981, Miyagi and Nishida, 1979).

Without pulse broadening, there is no pulse-to-pulse interaction. However, pulse broadening is not necessary bad for pulse-to-pulse interaction. From Eq. (7.3), the amplitude of the pulse decreases with pulse width. After sufficient pulse broadening, the effects of pulse-to-pulse interaction decrease accordingly.

For illustration purpose, for two optical pulses of

$$E_1(t) = A_0 e^{-t^2/2\tau^2}, \qquad E_2(t) = A_0 e^{-(t-T)^2/2\tau^2}, \tag{7.5}$$

with the same $1/e$ width of τ and separated by the time of T, the action of cross-phase modulation (XPM) from $E_2(t)$ to $E_1(t)$ can be described by $dE_1(t)/dz = j\gamma E_1(t)|E_2(t)|^2$. With a phase shift of $\gamma|E_2(t)|^2$, the instantaneous phase shift is $d\delta\phi_1(t)/dz = \gamma|E_2(t)|^2$ with a mean phase shift of

$$\frac{d\Delta\phi_1}{dz} = \frac{\int \frac{d\delta\phi_1(t)}{dz}|E_1(t)|^2 \mathrm{d}t}{\int |E_1(t)|^2 \mathrm{d}t}, \tag{7.6}$$

or

$$\frac{d\Delta\phi_1}{dz} = \frac{\gamma P_0}{\sqrt{2\pi}} \frac{T}{\tau} \exp\left(-\frac{T^2}{2\tau^2}\right), \tag{7.7}$$

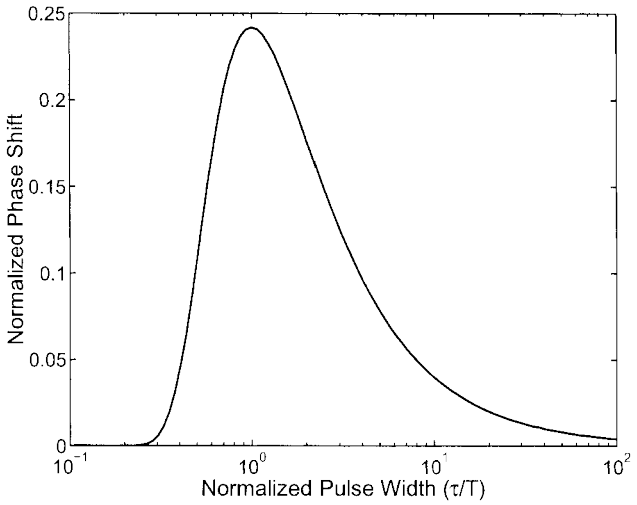

Figure 7.1. The normalized phase shift function as a function of τ/T

where the optical power of the pulse train is equal to

$$P_0 = \sqrt{\pi} A_0^2 \tau / T. \tag{7.8}$$

Figure 7.1 shows the function of $\frac{1}{\sqrt{2\pi}}(\tau/T)e^{-T^2/2\tau^2}$ from Eq. (7.7) as a function of τ/T. With no pulse overlap when $\tau \ll T$, there is also no phase shift as from Fig. 7.1. The phase shift is the largest at $\tau = T$ with moderated pulse overlap but decreases with the occurrence of further pulse overlap when $\tau \gg T$. Figure 7.1 shows two regions with small pulse-to-pulse interaction effect when τ is either much smaller or larger than the pulse separation of T.

In practical communication systems, a train of pulse is transmitted to carry information. Pulse broadening reduces the effect of each interacting component as from Fig. 7.1. However, two far away pulses with large time separation may also overlap with each other and gives more phase shift. Systems with large dispersion and fast pulse broadening may but not necessary provide better performance.

Intrachannel interaction in very dispersive fiber is first observed by Shake et al. (1998) and Essiambre et al. (1999). The reduction of intrachannel pulse-to-pulse interaction by pulse broadening was first proposed in Mamyshev and Mamysheva (1999). The derivation here follows the method of Mamyshev and Mamysheva (1999). As a comparison, in

soliton-to-soliton interaction, as shown in Gordon (1983), distortion increases monotonically with pulse overlap.

2. Intrachannel Four-Wave Mixing

The combination of fiber Kerr effect, fiber loss and dispersion can be described by the nonlinear Schrödinger equation of

$$\frac{\partial A}{\partial z} + \frac{j\beta_2}{2}\frac{\partial^2 A}{\partial z^2} + \frac{\alpha}{2}A = j\gamma|A|^2 A, \tag{7.9}$$

where $A(z,t)$ is the low-pass representation of the optical signal. At the location of z, assume that there are pulses of

$$u_k(z,t) = \frac{A_k T_0}{(T_0^2 - j\beta_2 z)^{1/2}} \exp\left[-\frac{(t-kT)^2}{2(T_0^2 - j\beta_2 z)}\right], \tag{7.10}$$

where $A_k = \{0, A_0\}$ for on-off keying and $A_k = \pm A_0$ for either phase-shift keying (PSK) or DPSK signal. The overall optical signal is $A(z,t) = e^{-\alpha z/2}\sum_k u_k(z,t)$.

The nonlinear force of $j\gamma|A|^2A$ for nonlinear Schrödinger equation is $F_0(z,t) = j\gamma u_l n_m u_n^* e^{-3\alpha z/2}$ when the pulses of u_l, u_m, and u_n are considered in $A(z,t) = u_l + u_m + u_n + \cdots$. Self-phase modulation (SPM) is induced to the pulse of u_l if $m = n = l$. SPM from $m = n = l$ is called intrachannel SPM (ISPM) in this chapter. Intrachannel cross-phase modulation (IXPM) is induced to the pulse of u_l when $m = n \neq l$ and the pulse of u_m when $l = n \neq m$. As shown later, intrachannel four-wave mixing (IFWM) is induced to the pulse of u_k if $k = l + m - n$, $l \neq n$, and $m \neq n$.

The nonlinear force term of $F_0(z,t)$ is equal to

$$F_0(z,t) = j\gamma A(z) \exp\left[-a(z)t^2 + b(z)Tt - c(z)T^2\right] \tag{7.11}$$

where

$$\begin{aligned} A(z) &= \frac{A_l A_m A_n^* T_0^3 e^{-3\alpha z/2}}{\sqrt{|\xi|^2 \xi}}, & a(z) &= \frac{1}{2}\left(\frac{1}{\xi^*} + \frac{2}{\xi}\right), \\ b(z) &= \frac{n}{\xi^*} + \frac{l+m}{\xi}, & c(z) &= \frac{1}{2}\left(\frac{n^2}{\xi^*} + \frac{l^2+m^2}{\xi}\right) \end{aligned} \tag{7.12}$$

with $\xi = T_0^2 - j\beta_2 z$. The Fourier transform of $F_0(z,t)$ is

$$\hat{F}_0(z,\omega) = j\gamma A(z)\sqrt{\frac{\pi}{a(z)}} \exp\left\{-c(z)T^2 - \frac{[\omega + jb(z)T]^2}{4a(z)}\right\}. \tag{7.13}$$

With large pulse overlap when $|\beta_2|z \gg T_0$, $\xi \sim -j\beta_2 z$ is close to a pure imaginary number, we obtain $b(z) \sim (l+m-n)/\xi$ and $a(z) \sim 1/2\xi$. Ignored some constant factors independent of ω, we obtain

$$\hat{F}_0(z,\omega) \sim \exp\left[-\frac{j}{2}\beta_2 z\omega^2 - j(l+m-n)\omega T\right]. \tag{7.14}$$

In time domain, the nonlinear force of $F_0(z,t)$ is centered at the time of $(l+m-n)T$, similar to four-wave mixing effects, the pulse width is equal to $\sqrt{|\beta_2|z/2}$.

The nonlinear force of $F_0(z,t)$ propagates for the remaining distance of $L-z$ to reach the destination of L. From the location of z to L, there is a fiber loss of $e^{-\alpha(L-z)/2}$, an optical amplifier with gain of $e^{\alpha L/2}$, and a dispersion compensator for an overall dispersion of $\beta_2 L$ for the whole fiber span, all located at the destination of L. At $z = L$, the nonlinear force of $\hat{F}_0(z,\omega)$ gives an electric field with Fourier transform of

$$\hat{F}_0(z,\omega)e^{-j\beta_2 z\omega^2/2}e^{\alpha z/2}. \tag{7.15}$$

For the whole fiber span from 0 to L, the overall nonlinear force in time domain is accumulated to

$$\Delta u_{l,m,n}(L,t) = \int_0^L \mathcal{F}_\omega^{-1}\left\{\hat{F}_0(z,\omega)e^{-j\beta_2 z\omega^2/2}\right\}e^{\alpha z/2}\mathrm{d}z, \tag{7.16}$$

where $\mathcal{F}_\omega^{-1}$ denotes inverse Fourier transform with respect to ω. We obtain

$$\begin{aligned}\mathcal{F}_\omega^{-1}\left\{\hat{F}_0(z,\omega)e^{-j\beta_2 z\omega^2/2}\right\} &= \frac{j\gamma A(z)}{\sqrt{1+2j\beta_2 z a(z)}} \\ &\times \exp\left\{-\frac{a(z)t^2 - b(z)Tt - jb^2(z)\beta_2 z/2}{1+2j\beta_2 z a(z)} - c(z)T^2\right\}. \end{aligned}\tag{7.17}$$

The above electric field can be simplified for $k = l+m-n$ in the general case. With a constant time shift, when $l+m-n = 0$ for the ghost pulses that affect $u_0(z,t)$ at $t = 0$, after some simplifications, we

obtain

$$\Delta u_{l,m,l+m}(L,t) = j\gamma A_l A_m A_{l+m}^* \exp\left(-\frac{t^2}{6T_0^2}\right) \times \int_0^L \frac{e^{-\alpha z}}{\sqrt{1+2j\beta_2 z/T_0^2+3(\beta_2 z/T_0^2)^2}} \times \exp\left\{-\frac{3(2t/3-lT)(2t/3-mT)}{T_0^2+3j\beta_2 z} - \frac{(m-l)^2T^2}{T_0^2\left[1+2j\beta_2 z/T_0^2+3(\beta_2 z/T_0^2)^2\right]}\right\}. \tag{7.18}$$

Unlike on-off keying, both PSK and DPSK signals are a constant pulse train as shown in Fig. 2.17. IXPM is induced to u_0 if $l = n, m = 0$ or $m = n, l = 0$, i.e., either $l = 0$ or $m = 0$. Assume that $l = 0$, the factor outside of the integration in Eq. (7.18) is $j\gamma A_0|A_m|^2$, i.e., a phase modulation proportional to $\gamma|A_m|^2$. While A_m induced phase modulation to u_0, A_{m+1} induces phase modulation to u_1. Because $|A_m|^2$ and $|A_{m+1}|^2$ has the same intensity of $|A_0|^2$ for PSK and DPSK signals, the phase difference between adjacent pulses u_0 and u_1 does not change due to IXPM. However, for on-off keying, there is 1/4 probability that $|A_m|^2 = |A_0|^2$ but $|A_{m+1}|^2 = 0$. In this particular case, the phase modulation changes the frequency of the pulse of u_0 but not u_1. Combined with chromatic dispersion of the fiber, the frequency modulation of on-off keying signal is translated to timing jitter. For phase-modulated signal, the timing jitter for all pulses is the same, i.e., no timing jitter variation. The timing jitter for on-off keying signal was considered in Ablowitz and Hirooka (2001, 2002), Kumar et al. (2002), Mårtensson et al. (2001), and Mecozzi et al. (2000a,b, 2001). IXPM does not degrade the DPSK signals. Similarly, ISPM also does not degrade DPSK signals.

The pulse-to-pulse interaction is small if optical pulses do not overlap. Significant interaction occurs only when $|\beta_2|z/T_0^2 \gg 1$. In this limit and for lossless fiber with $\alpha = 0$, we obtain

$$\Delta u_{l,m,l+m}(L,t) = j\gamma A_l A_m A_{l+m}^* e^{-t^2/6T_0^2} \frac{T_0^2}{\sqrt{3}|\beta_2|} E_1\left(-j\frac{lmT^2}{\beta_2 L}\right), \tag{7.19}$$

where $E_1(x) = \int_1^{+\infty} t^{-1}e^{-xt}\mathrm{d}t$ is the exponential integral (Gradshteyn and Ryzhik, 1980, §8.21). From Eq. (7.19), the pulse induced from the nonlinear force is Gaussian shape with a pulse width of $\sqrt{3}T_0$. From the channel power of Eq. (7.8), the pulse amplitude of Eq. (7.19) to A_0 is

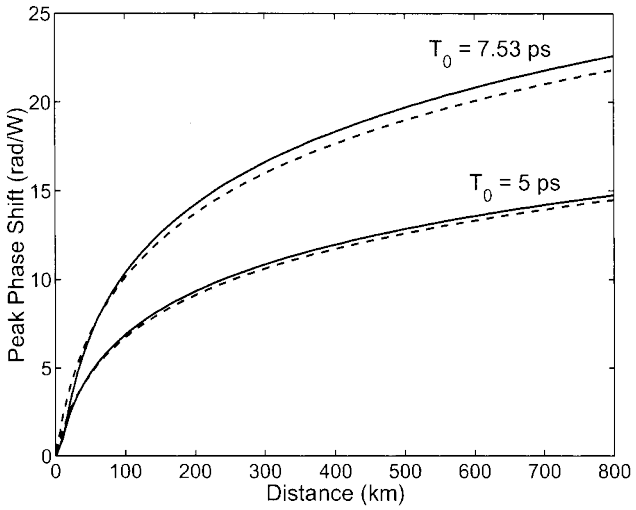

Figure 7.2. The peak phase shift due to IFWM as a function of distance for lossless fiber. The solid lines are the exact integration of Eq. (7.18) and the dashed lines are the approximation of Eq. (7.19).

proportional to P_0T_0, or

$$\frac{\Delta u_{l,m,l+m}(L,0)}{A_0} \propto P_0T_0. \tag{7.20}$$

The amplitude variation is proportional to the pulse width. With shorter pulse, the pulse width increases very fast due to fiber chromatic dispersion. The ghost pulses from IFWM reduce accordingly. The usage of short optical pulse in highly dispersive transmission reduces IFWM induced ghost pulses.

Figure 7.2 shows the peak phase shift of $2\Delta u_{+1,-1,0}/A_0$ due to the two degenerated IFWM from $l = +1, m = -1$ and $l = -1, m = +1$. The peak phase shift is expressed in the unit of rad/W for a pulse width of $T_0 = 7.53$ and 5 ps, and the bit interval of $T = 25$ ps for 40-Gb/s system. The fiber nonlinear coefficient is $\gamma = 1.24$/km/W. The group-velocity dispersion coefficient is $\beta_2 = -21.7$ ps^2. For lossless fiber, Figure 7.2 shows that the approximation of Eq. (7.19) is very close to the integration of Eq. (7.18). From Fig. 7.2, the amount of IFWM also increases with the initial pulse width of T_0.

3. Impact to DPSK Signals

Although IXPM does not affect DPSK signals and is excluded here right now, IFWM gives ghost pulses exactly located at the signal pulse. In the simplest model, the ghost pulse can be modeled as Gaussian noise although numerical simulation shows a distribution having significant different with Gaussian distribution. This section first studies the statistical properties of IFWM. The error probability of DPSK signals with IFWM is evaluated based on both empirical Gaussian approximation and a semi-analytical model.

3.1 Statistics of Intrachannel Four-Wave Mixing

When many pulses in the fiber are interacted with each other through IFWM, the overall IFWM induced ghost pulses have a peak amplitude of

$$\begin{aligned} \Delta u_0 &= \sum_{l,m,l\neq 0,m\neq 0} \Delta u_{l,m,l+m}(L,0), \\ \Delta u_1 &= \sum_{l,m,l\neq 1,m\neq 1} \Delta u_{l,m,l+m-1}(L,0) \end{aligned} \tag{7.21}$$

co-located with u_0 and u_1 at $t = 0$ and $t = T$, respectively. If N_A identical fiber spans with a length of L are used repeatedly one after another, IFWM adds coherently one span after another. The overall IFWM ghost pulse has a peak amplitude N_A times that of Eq. (7.21), or equivalently speaking, induced by a single-span fiber link with a launched power of $N_A P_0$. In practice, the repetition of identical fiber span gives the largest accumulation of fiber nonlinearities, representing the worst-case system design. For a fiber link with arbitrary configuration, each ghost pulse of $\Delta u_{l,m,l+m}$ can be calculated using N_A different integrations of Eq. (7.18).

Figure 7.3(a) shows the distribution of the peak normalized electric field of $\Delta u_0/A_0$. Figure 7.3(b) shows the distribution of the peak relative phase shift of $\Im\{\Delta u_0\}/A_0$ versus $\Im\{\Delta u_1\}/A_1$ between two consecutive time intervals, where $\Im\{\cdot\}$ denotes the imaginary part of a complex number. Figure 7.3(c) shows the distribution of $\Re\{\Delta u_0\}/A_0$ versus $\Re\{\Delta u_1\}/A_1$ between two consecutive time intervals, where $\Re\{\cdot\}$ denotes the real part of a complex number. Figures 7.3 are obtained for 100-km long fiber span with a normalized launched power of $\langle \Phi_{\mathrm{NL}} \rangle = N_A \gamma L_{\mathrm{eff}} P_0 = 1$ rad, 100% dispersion compensation at the end of each fiber link. The fiber link has an attenuation coefficient of $\alpha = 0.2$ dB/km. The pulse width is $T_0 = 7.53$ ps, corresponding to a FWHM pulse width of 12.5 ps, or 50% of the bit interval of $T = 25$ ps for 40-Gb/s DPSK signals. The distributions of Figs. 7.3 are shown as a gray scale inten-

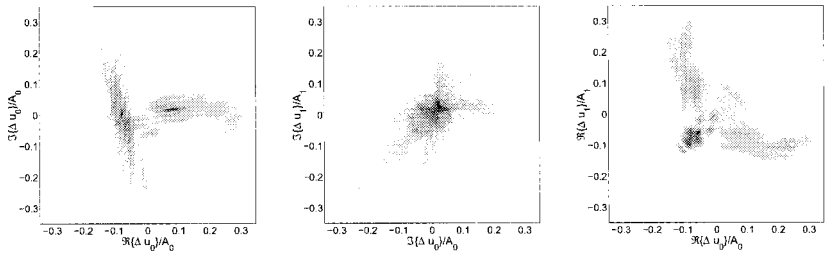

Figure 7.3. Distribution of IFWM ghost pulses. (a) The distribution of the complex electric field of $\Delta u_0/A_0$. (b) The distribution of the relative phase of $\Im\{\Delta u_0\}/A_0$ versus $\Im\{\Delta u_1\}/A_1$ for two consecutive symbols. (C) The distribution of the real parts of the electric field of $\Re\{\Delta u_0\}$ versus $\Re\{\Delta u_1\}/A_1$ for two consecutive symbols.

sity. The simulation of Figs. 7.3 uses 20-bit DPSK signal with about 1 million different combinations. Figure 7.3(a) is for ghost pulse at the center bit and Fig. 7.3(b) is the imaginary parts of the ghost pulses of the two center bits. If the ghost pulses have peak amplitude significantly smaller than the pulse amplitude of $|A_0|$, Figure 7.3(b) is approximately the relative phase shift between two consecutive pulses, i.e., the x-axis is $\Im\{\Delta u_0\}/A_0$ and the y-axis is $\Im\{\Delta u_1\}/A_1$. The simulation of Figs. 7.3 ignores all the contribution from ISPM and IXPM that do not degrade DPSK signals. When identical fiber span is repeated one after another, IFWM induced ghost pulses add coherently one after another. Figures 7.3 are valid for single- and multi-span fiber link with mean nonlinear phase shift of $\langle \Phi_{\mathrm{NL}} \rangle = 1$ rad.

From Figs. 7.3, the IFWM induced ghost pulse does not have a regular distribution. While the imaginary part in Fig. 7.3(a) has larger peak amplitude, the real part of the ghost pulse is still very significant and has twice the variance of the imaginary part. Although $\Delta u_0/A_0$ is zero mean, the distribution of Fig. 7.3(a) trends toward positive real part but spreads more or less equally in both positive and negative imaginary part.

The IFWM ghost pulses induce phase changes of $\Im\{\Delta u_0\}/A_0$ and $\Im\{\Delta u_1\}/A_1$ that are correlated with each other. The correlation coefficient of that in Fig. 7.3(b) is about 0.58. The positive correlation reduces the impact of IFWM to the error probability of DPSK signal. As adjacent pulses trend to have similar phase shift, the phase difference is reduced accordingly.

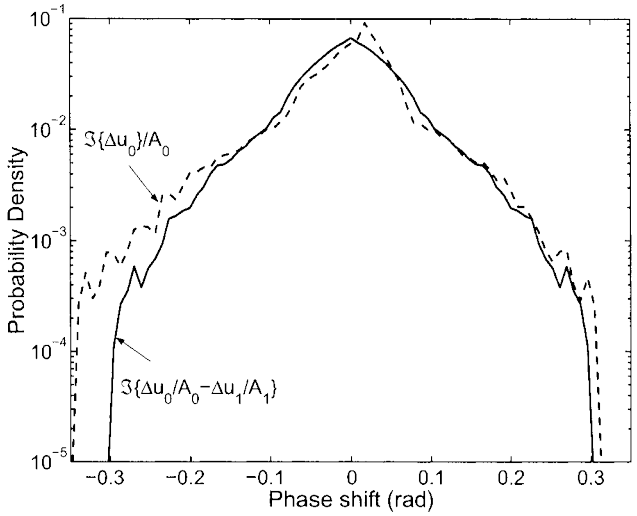

Figure 7.4. The phase distribution of IFWM.

The real part correlation of Fig. 7.3(c) is different with the correlation of Fig. 7.3(b) for imaginary part. If $\Re\{\Delta u_0\}/A_0$ is very large and positive, $\Re\{\Delta u_1\}/A_1$ is usually very small. The correlation coefficient is negative and equal to about -0.55. When the real part of $\Re\{\Delta u_0\}/A_0$ mostly has large positive values but $\Re\{\Delta u_1\}/A_1$ has small value, the error probability reduces as the two constellation points of two consecutive symbols are further apart. The correlation property of Fig. 7.3(c) also reduces the error probability for DPSK signal.

When A_k all change sign to $-A_k$, $\Delta u_0/A_0$ remains the same. The ghost pulses of Δu_0 is symmetrical with the origin and equal to that in Fig. 7.3(a) and its rotation by 180° for negative A_0. When A_k is changed to $(-1)^k A_k$ with sign change in only odd position, Δu_0 remains the same but Δu_1 changes sign. However, $\Im\{\Delta u_0\}/A_0$ and $\Im\{\Delta u_1\}/A_1$ remains the same. The distribution of $\Im\{\Delta u_0\}$ versus $\Im\{\Delta u_1\}$ is the 90°, 180°, and 270° rotations of Fig. 7.3(b).

Figure 7.4 shows the phase distribution due to IFWM, including the phase shift of $\Im\{\Delta u_0\}/A_0$ and the phase difference of $\Im\{\Delta u_0\}/A_0 - \Im\{\Delta u_1\}/A_1$. Figure 7.4 is shown for the same parameters of Figs. 7.3. Numerical calculation shows the variance of the IFWM-induced phase difference of $\Im\{\Delta u_0\}/A_0 - \Im\{\Delta u_1\}/A_1$ is about the same as the variance of the phase of $\Im\{\Delta u_0\}/A_0$, showing that the phase shift at two consecutive symbols are correlated with each other.

The distribution of Fig. 7.3(b) is basically the same as that in Wei and Liu (2003, Fig. 2). The distribution of Fig. 7.4 is also similar to that in Wei and Liu (2003, Fig. 3). For Figs. 7.3, we consider a fiber with loss instead of the lossless case of Wei and Liu (2003). For lossy fiber with span-by-span dispersion compensation, ghost pulses from IFWM are not reduced by 50% precompensation of chromatic dispersion. IFWM can be reduced by dispersion management, usually using symmetric dispersion compensation (Mecozzi et al., 2001, Striegler and Schmauss, 2004). However, the compensation scheme of Mecozzi et al. (2001) does not use dispersion management along the fiber, similar to the recent system demonstration of Vaa et al. (2004) with lump dispersion compensation at the beginning and end of the fiber link.

3.2 Error Probability for DPSK Signals

The error probability of DPSK signal with IFWM ghost pulse is difficult to find analytically. From Figs. 7.3, the distribution of the IFWM induced ghost pulses is not Gaussian distributed. Of course, similar to the simulated error probability of Figs. 5.10 and 5.14, the impact of IFWM to DPSK signal can be studied based on numerical simulation. However, with the distribution of Fig. 7.3 evaluated numerically, the error probability of DPSK signal with IFWM can be calculated semi-analytically.

Similar to the approaches of Secs. 3.4.2 and 4.2, ignored the constant factor of interferometer loss and photodiode responsivity, the photocurrent is

$$i(t) = |E(t) + \Delta u_1 + E(t-T) + \Delta u_0|^2 - |E(t) + \Delta u_1 - E(t-T) - \Delta u_0|^2, \tag{7.22}$$

where Δu_0 and Δu_1 are ghost pulses due to IFWM, located at two consecutive time intervals of $t = 0$ and $t = T$, respectively. Assumed for simplicity that the transmitted phases at $t = 0$ and $t = T$ are identical and, without loss of generality, $E_s(t) = E_s(t-T) = A_0 > 0$. With $E(t) = A_0 + n(t)$, we obtain

$$i(t) = |2A_0 + \Delta u_1 + \Delta u_0 + n(t) + n(t-T)|^2 - |\Delta u_1 - \Delta u_0 + n(t) - n(t-T)|^2. \tag{7.23}$$

A decision error occurs if $i(t) < 0$. Given Δu_0 and Δu_1, the two terms of Eq. (7.23) are independent of each other and have a noncentral chi-square (χ^2) distribution. Each term of Eq. (7.23) has the same noise variance of $4\sigma_n^2$ where $E\{|n(t)|^2\} = 2\sigma_n^2$. The noncentralities of two terms of Eq. (7.23) are $|2A_0 + \Delta u_1 + \Delta u_0|^2$ and $|\Delta u_1 - \Delta u_0|^2$, respectively.

From Appendix 3.A, the probability of $i(t) < 0$ is equal to

$$p_e(\Delta u_0, \Delta u_1) = Q(a, b) - \frac{1}{2} e^{-(a^2+b^2)/2} I_0(ab), \tag{7.24}$$

where

$$a^2 = \frac{\rho_s}{2} \left| 2 + \frac{\Delta u_1}{A_0} + \frac{\Delta u_0}{A_0} \right|^2, \tag{7.25}$$

$$b^2 = \frac{\rho_s}{2} \left| \frac{\Delta u_1}{A_0} - \frac{\Delta u_0}{A_0} \right|^2, \tag{7.26}$$

where $\rho_s = A_0^2/2\sigma_n^2$ is the signal-to-noise ratio (SNR) without taking into account the ghost pulses.

The error probability is equal to the expectation of

$$p_e = E\left\{p_e(\Delta u_0, \Delta u_1)\right\} \tag{7.27}$$

that can be evaluated numerically based on the distribution of, for example, Figs. 7.3. From the distribution of Figs. 7.3(b) and (c), when $|\Delta u_0|$ is very large, $|\Delta u_1|$ is also very large too. When $\Delta u_0 + \Delta u_1$ has its peak values, either positive or negative, $\Delta u_0 - \Delta u_1$ is usually very small. Similarly, when $\Delta u_0 - \Delta u_1$ has its peak values, $\Delta u_0 + \Delta u_1$ is usually very small. The error probability of Eq. (7.27) only considers the case when $A_0 = A_1$. As discussed above, the distribution for $A_0 = -A_1$ of the ghost pulses for Figs. 7.3(b) and (c) are the same as that for $A_0 = A_1$. If the transmitted symbols of two consecutive symbols have a phase difference of 180°, the error probability is the same as that given by Eq. (7.27) for $A_0 = A_1$ without phase difference.

For the real parts of the ghost pulses of $\Delta u_0/A_0$ and $\Delta u_1/A_1$, the correlation coefficient is negative, giving a variance of $\Re\{\Delta u_0\}/A_0 - \Re\{\Delta u_1\}/A_0$ larger than the variance of $\Re\{\Delta u_0\}/A_0 + \Re\{\Delta u_1\}/A_0$. The negative correlation supposes to increase the error probability. However, from Fig. 7.3(c), when $\Re\{\Delta u_0\}/A_0$ has large positive values, $\Re\{\Delta u_1\}/A_1$ has small value, the error probability reduces as the two constellation points of two consecutive symbols are further apart. The combined effect of negative correlation but special distribution should reduce the effect of IFWM ghost pulses to error probability.

Figure 7.5 shows the error probability as a function of SNR ρ_s for DPSK signal with IFWM induced ghost pulses. The semi-analytical formula of Eq. (7.27) with (7.26) is used to calculate the error probability based on IFWM ghost pulses distribution of Figs. 7.3 from a 16-bit permutation of a binary sequence. The number of bits is reduced for Fig. 7.5 as large number of bits increases the computation time but

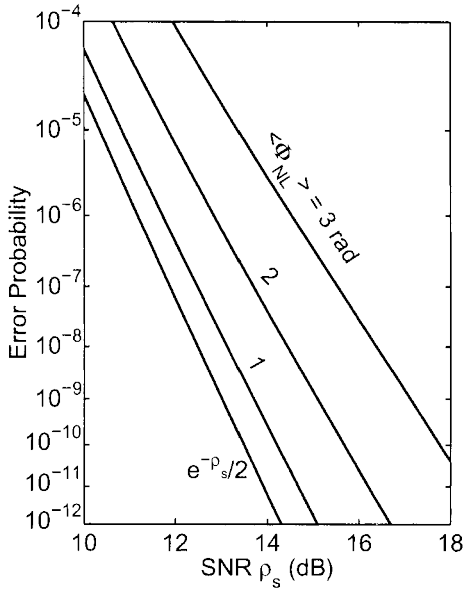

Figure 7.5. The error probability as a function of SNR for DPSK signal with IFWM induced ghost pulses.

not the accuracy of the curves in Fig. 7.5. The system configuration is the same as that for Figs. 7.3. The mean nonlinear phase shift is $\langle \Phi_{\rm NL} \rangle = N_A \gamma L_{\rm eff} P_0$. Assume that identical fiber span is repeated one after another, Figure 7.5 is valid for single and multiple systems with the same $\langle \Phi_{\rm NL} \rangle$. Of course, the repeat of the same configuration span after span is the worst-case with the largest accumulation of distortion due to fiber nonlinearities.

Figure 7.6 shows the SNR penalty as a function of mean nonlinear phase shift $\langle \Phi_{\rm NL} \rangle$. In additional to the SNR penalty corresponding to Fig. 7.5, Figure 7.6 also shows the SNR for the case when the initial pulse width is $T_0 = 5$ ps, for a duty cycle of about 1/3. Followed the estimation of Fig. 7.2, a system with short initial pulse width has less IFWM and smaller IFWM induced SNR penalty.

If the IFWM induced ghost pulses are assumed as Gaussian distributed electric field, the noise is increased to $n(t) + \Delta u_0$ at $t = 0$. The SNR including the ghost pulse has a SNR ratio of $A_0^2 / E\{|n(t) + \Delta u_0|^2\}$. However, this definition of SNR ignores the correlation between Δu_0 and Δu_1.

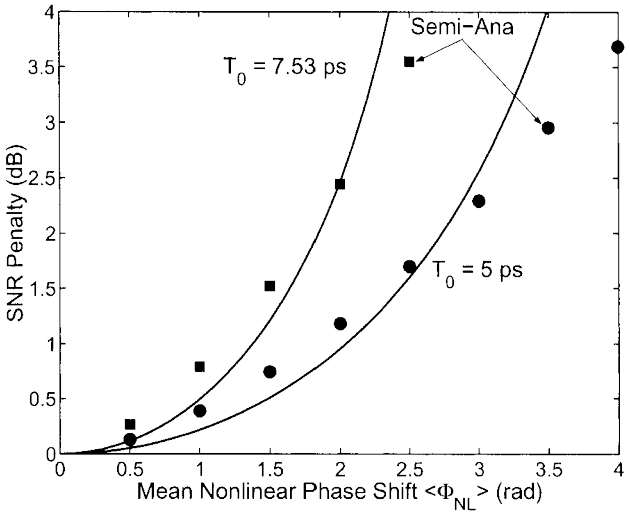

Figure 7.6. The SNR penalty as a function of mean nonlinear phase shift of $\langle \Phi_{\mathrm{NL}} \rangle$. [Adapted from Ho (2005c)]

The variance of the phase of $A_0 + n(t)$ is approximately equal to $1/2\rho_s$ from Eq. (4.A.15). Similar to that for the Q-factor of Eq. (5.81), the differential phase has a phase variance of $1/\rho_s$. For IFWM induced ghost pulses, the corresponding differential phase variance is

$$\sigma_{\Delta\phi}^2 = E\left\{ \left[\Im\{\Delta u_0\}/A_0 - \Im\{\Delta u_1\}/A_1 \right]^2 \right\}. \tag{7.28}$$

With this additional differential phase variance, the SNR penalty can be estimated as

$$-10 \cdot \log_{10}\left(1 - 20\sigma_{\Delta\phi}^2\right), \tag{7.29}$$

where 20 (13 dB) is the required SNR to give an error probability of 10^{-9} for DPSK signal as from Fig. 3.13.

Figure 7.6 also shows the SNR penalty calculated by Eq. (7.29). For a SNR penalty less than 2 dB, the SNR penalty of Eq. (7.29) underestimates the SNR penalty by up to 0.25 dB. For SNR penalty larger than 2 dB, the SNR penalty of Eq. (7.29) overestimates the SNR penalty.

Note that the usage of the approximation of Eq. (7.29) does not greatly simplify the analysis of DPSK signal with IFWM induced ghost pulses. To calculate the variance of $\sigma_{\Delta\phi}^2$ of Eq. (7.28), IFWM terms of Δu_0 induce by many different combinations of bit sequence must be evaluated. The semi-analytical error probability just requires one further step to find the error probability of Eq. (7.26) for each combination

of Δu_0 and Δu_1. The average error probability of Eq. (7.27) becomes the error probability for the system. The variance of Eq. (7.29) in different mean nonlinear phase shift of $\langle \Phi_{\mathrm{NL}} \rangle$ increases with $\langle \Phi_{\mathrm{NL}} \rangle^2$. The whole curves of Fig. 7.6 requires, to certain extend, one evaluation of the variance of $\sigma^2_{\Delta\phi}$. However, using the same set of $\Delta u_0/A_0$ and $\Delta u_1/A_1$, different point of the semi-analytical results in Fig. 7.6 requires the evaluation of a new set of error probabilities of Eq. (7.26) to find the average of Eq. (7.27).

The above analysis and numerical results always used the peak amplitude of the ghost pulses and the signal pulses. The pulse width of the ghost pulses is ignored for simplicity. However, the IFWM terms of Eq. (7.18) does not have the same pulse shape as the signal but in fact approximately broadens to $\sqrt{3}$ times wider than the signal. As the power is proportional to the pulse width, the ghosts pulse has $\sqrt{3}$ times larger power than the signal. In the worst case, the corresponding curves of Fig. 7.6 must be scaled by a factor of $3^{1/4} = 1.32$ to take that into account. However, the discrepancy due to pulse width depends on the bandwidth of the optical and electric filters in the receiver.

If optical matched filter is used preceding the polarized direct-detection DPSK receiver and the electric filter at the receiver has a wide bandwidth that does not distort the signal, assume the ghost pulse is $\sqrt{3}$ times wider than the signal pulse, the IFWM amplitude is increased by a factor of $\sqrt{3/2} = 1.22$, less than the ratio of $3^{1/4}$ due to power increase.

If both the optical and electric filter has a very wide bandwidth, a very bad case that allows too much noise to the receiver, the peak amplitude directly transfers to the receiver. IFWM does not increase from the peak amplitude for Eq. (7.18). If the optical filter has a wide bandwidth but the electrical filter is a Bessel filter having a bandwidth 0.75 time the data rate, IFWM increases by a factor of 1.19 relative to the signal pulse.

In practical system design, Figure 7.6 must be modified to take into account the design of both receiver and transmitter. Also note that the results of this section assume an optical matched filter but ignored the pulse width of ghost pulses.

IFWM and IXPM were first observed by Shake et al. (1998), and Essiambre et al. (1999) and first analyzed by Mamyshev and Mamysheva (1999). The analysis here follows similar method in Ablowitz and Hirooka (2002), Mecozzi et al. (2000b), Striegler and Schmauss (2004), and Wei and Liu (2003). The formula of Eq. (7.18) was first derived in Mecozzi et al. (2001) but modified by Essiambre et al. (2002) and Chowdhury and Essiambre (2004).

IFWM can be suppressed using symmetric dispersion compensation (Mecozzi et al., 2001, Striegler and Schmauss, 2004, Wei and Plant,

2004) and alternating polarization (Liu et al., 2004c, Xie et al., 2004). As a general method, optical phase conjugation can also reduce IFWM (Brener et al., 2000, Chowdhury and Essiambre, 2004, Chowdhury et al., 2005, Pepper and Yariv, 1980).

While phase modulation is another method to suppress IFWM for on-off keying (Alic and Fainman, 2004, Appathurai et al., 2004, Cheng and Conradi, 2002, Forzati et al., 2002, Gill et al., 2003, Liu et al., 2002a), DPSK signal always has phase modulation with higher tolerance to IFWM than on-off keying signal. For on-off keying signal, all terms of $A_l A_m A_{l+m}^*$ are positive and sum together. With phase modulation, the factors of $A_l A_m A_{l+m}^*$ may be positive and negative. Of course, if the terms of $A_l A_m A_{l+m}^*$ for different l and m are independent of each other, the variance of the ghost pulse remains the same as the case without phase modulation. However, because of the dependence between terms for different l and m, the overall IFWM reduces by phase modulation. Phase modulation is intrinsically used in DPSK signals and IFWM can thus be reduced accordingly.

IXPM also dose not degrade PSK signal as the phase-locked loop (PLL) tracks out the constant phase. Like usual PSK signal receiver, if the demodulator of PSK signal does not take into account the correlation between two adjacent ghost pulses. The SNR penalty for PSK signal is larger than that for DPSK signal and performs worst than DPSK signal in high IFWM. Using a method similar to Eq. (7.29), the SNR penalty for PSK signal can be estimated as

$$-10 \cdot \log_{10}\left(1 - 36E\left\{\left[\Im\{\Delta u_0/A_0\}\right]^2\right\}\right). \tag{7.30}$$

When the phase variance and the differential phase variance is approximately the same from Fig. 7.4, the SNR penalty for PSK signal may be larger than that for DPSK signals. Of course, practical PSK receiver may be designed to anticipate the correlate phase due to IFWM. In practice, the phase error for PSK signal must be analyzed based on Eq. (4.26) for a phase-locked loop with closed-loop transfer function of $H(s)$. The correlation of IFWM ghost pulses must be included in $S_{\phi_n}(f)$ for Eq. (4.26). Currently, the power spectral density of the IFWM ghost pulses is not known.

4. Nonlinear Phase Noise Versus Intrachannel Four-Wave-Mixing

The previous Chapters 5 and 6 all consider non-return-to-zero (NRZ) signals without pulse distortion when the optical signal is propagated through the optical fiber. In Sec. 5.1, the mean nonlinear phase shift for an optical pulse is given by Eq. (5.8) for NRZ or continuous-wave signal.

However, SPM induced nonlinear phase noise for short pulse requires special treatment other than the method in Chapter 5, especially must be consistent with previous section for a fair comparison with IFWM.

The mean nonlinear phase shift of $\langle \Phi_{\rm NL} \rangle = \gamma N_A P_0 L_{\rm eff}$ does not change with signal format of RZ-OOK or RZ-DPSK. ISPM phase noise, or SPM-induced nonlinear phase noise, is given by the beating of the optical pulse itself with amplifier noises. For system without chromatic dispersion, for the same average power, the peak amplitude of the signal is inversely proportional to the pulse width. In additional to giving more nonlinear phase noise to the signal, the usage of RZ pulse gives time-dependence to the nonlinear phase noise. The variance of nonlinear phase noise is a function of time and the peak variance of nonlinear phase noise increases with the decrease of pulse width.

For system with chromatic dispersion, from Eq. (7.3), the optical pulse broadens with transmission distance. The pulse is usually broadened faster for shorter pulse. Nonlinear phase noise decreases with chromatic dispersion, mostly due to pulse broadening. With pulse overlap, the adjacent pulses beat with the amplifier noise located with the center pulse. IXPM phase noise, or IXPM-induced nonlinear phase noise, increases with pulse broadening. As shown later, the combined ISPM and IXPM phase noises are comparable to the nonlinear phase noise of NRZ signal without pulse broadening.

To be consistent with the method to derive Eq. (7.18), we consider the nonlinear force of the interaction of signal with noise. For signal with amplifier noise, the SPM-induced nonlinear force including amplifier noises is equal to

$$j\gamma[u_0(z,t)+n(z,t)]|u_0(z,t)+n(z,t)|^2. \tag{7.31}$$

The nonlinear force for ISPM is $j\gamma u_0|u_0|^2$ from the signal alone, the same as that for Eq. (7.18) with $l = m = 0$. The nonlinear force associated with nonlinear phase noise has two different terms of

$$2j\gamma|u_0(z,t)|^2 n(z,t), \quad \text{and} \quad j\gamma u_0^2(z,t)n^*(z,t), \tag{7.32}$$

when all quadratic or higher-order terms of the noise are ignored at high SNR. The IXPM term of $2j\gamma|u_m(z,t)|^2 n(z,t)$ also gives IXPM phase noise to the pulse of $u_0(z,t)$ at $t = 0$. For system with large SNR, the IFWM related noise and signal beating of $2j\gamma u_l(z,t)u_m^*(z,t)n(z,t)$ with $l \neq m$ is much smaller than the IFWM induced ghost pulses from the same effects. While IFWM phase noise is ignored, the ISPM phase noise is considered but its result is also applicable to IXPM phase noise, almost without modification. As shown in last section, pulse-to-pulse interaction due to both ISPM and IXPM gives the same phase shift

to all pulses and does not degrade a DPSK signal. While the pulse-to-pulse interaction due to IFWM gives ghost pulses, both ISPM and IXPM phase noises are from the interaction of pulses with amplifier noises. Due to the difference of amplifier noise located at adjacent pulses, ISPM and IXPM phase noises are not the same at adjacent pulses.

For the nonlinear force from $2j\gamma|u_0(z,t)|^2 n(z,t)$, the overall nonlinear force is equal to

$$\Delta u_n(t) = 2j\gamma \int_0^L \left[|u_0(z,t)|^2 n(z,t)\right] \otimes h_{-z}(t) e^{-\alpha z} \mathrm{d}z, \tag{7.33}$$

where $\otimes$ denotes convolution. The impulse response of $h_{-z}(t)$ provides dispersion compensation for $h_z(t)$, where $h_z(t)$ is an impulse response from fiber chromatic dispersion, the corresponding transfer function is $H_z(\omega) = \exp(j\beta_2 z\omega^2/2)$.

Due to fiber chromatic dispersion, from Eq. (7.3), the pulse of $|u_0(z,t)|^2$ has an $1/e$ width of $\tau(z)/\sqrt{2}$ and a Fourier transform of

$$V_0(z,\omega) = \sqrt{\pi}|A_0|^2 T_0 \exp\left[-\tau^2(z)\omega^2/4\right], \tag{7.34}$$

where $\tau(z)$ is the pulse width as a function of distance given by Eq. (7.4). The optical amplifier noise of $n(z,t)$ is also changed due to fiber dispersion. Although fiber dispersion does not change the spectrum of the signal, the time dependence of the signal is changed by chromatic dispersion. At the input of the fiber, $E\{n(0,t+\tau)n^*(0,t)\} = 2\sigma_n^2\delta(\tau)$ as additive white Gaussian noise, where σ_n^2 is the noise variance per dimension. With fiber dispersion, $n(z,t) = n(0,t) \otimes h_z(t)$ and $E\{n(z,t+\tau)n(z,t)\} = 2\sigma_n^2\delta(\tau)$, but

$$\begin{aligned}\int_{-\infty}^{+\infty} E\{n(z_1,t+\tau)n^*(z_2,t)\} e^{-j\omega\tau}\mathrm{d}\tau \\ = 2\sigma_n^2 H_{z_1}(\omega)H_{z_2}^*(\omega) = 2\sigma_n^2 e^{j\beta_2(z_1-z_2)\omega^2/2}.\end{aligned} \tag{7.35}$$

The temporal profile of $\Delta u_n(t)$ can be represented by the variance of $\Delta u_n(t)$ as a function of time, or

$$\begin{aligned}\sigma^2_{\Delta u_n}(t) &= E\left\{|\Delta u_n(t)|^2\right\} \\ &= 4\gamma^2 \int_0^L \int_0^L \int_{-\infty}^{+\infty} \int_{-\infty}^{+\infty} |u_0(z_2,\tau_2)|^2 |u_0(z_1,\tau_1)|^2 \\ &\quad \times E\{n(z_1,\tau_1)n^*(z_2,\tau_2)\} h^*_{-z_2}(t-\tau_2) h_{-z_1}(t-\tau_1) \\ &\quad \times e^{-\alpha z_1 - \alpha z_2} \mathrm{d}\tau_1 \mathrm{d}\tau_2 \mathrm{d}z_1 \mathrm{d}z_2.\end{aligned} \tag{7.36}$$

Replacing $E\{n(z_1,\tau_1)n^*(z_2,\tau_2)\}$, $h_{-z_1}(t)$, and $h_{-z_2}(t)$ with their corresponding Fourier transforms, we obtain

$$\sigma^2_{\Delta u_n}(t) = \frac{\gamma^2\sigma_n^2}{\pi^3}\int_0^L\int_0^L\int_{-\infty}^{+\infty}\int_{-\infty}^{+\infty}\int_{-\infty}^{+\infty} V_0(z_1,\omega_1-\omega)V_0(z_2,\omega_2-\omega) \times e^{j\beta_2(z_1-z_2)\omega^2/2}H^*_{-z_2}(\omega_2)H_{-z_1}(\omega_1) \times e^{j(\omega_1-\omega_2)t-\alpha(z_1+z_2)}\mathrm{d}\omega_1\mathrm{d}\omega_2\mathrm{d}\omega\mathrm{d}z_1\mathrm{d}z_2. \quad (7.37)$$

Note that both $V_0(z,\omega)$ and $H_z(\omega)$ are "Gaussian" shape and the integrations over z_1 and z_2 are complex conjugate of each other, the time-depending variance is equal to

$$\sigma^2_{\Delta u_n}(t) = \frac{4\gamma^2\sigma_n^2T_0^2A_0^4}{\pi}\int_{-\infty}^{+\infty}\left|\int_0^L \frac{\exp\left(-\frac{t^2+j\tau^2(z)\omega t+\beta_2^2z^2\omega^2}{\tau^2(z)-2j\beta_2z}-\alpha z\right)}{\sqrt{\tau^2(z)-2j\beta_2z}}\mathrm{d}z\right|^2\mathrm{d}\omega. \quad (7.38)$$

Similarly, the variance profile corresponding to $\gamma u_0^2(z,t)n^*(z,t)$ can be calculated by replacing $\tau^2(z)$ by $T_0^2 - j\beta_2 z$ and the spectral density for $n^*(z,t)$ is the complex conjugate of that for $n(z,t)$. We obtain

$$\sigma^2_{\Delta u_n'}(t) = \frac{\gamma^2\sigma_n^2T_0^2A_0^4}{\pi}\int_{-\infty}^{+\infty}\left|\int_0^L \frac{\exp\left[-\frac{(t-\beta_2z\omega)(t-jT_0^2\omega)}{T_0^2+j\beta_2z}-\alpha z\right]}{\sqrt{T_0^4+\beta_2^2z^2}}\mathrm{d}z\right|^2\mathrm{d}\omega. \quad (7.39)$$

Figure 7.7 shows the temporal profile, both the standard deviation (STD) of $\sigma_{\Delta u_n}(t)$ and $\sigma_{\Delta u_n'}(t)$, of the nonlinear force of both $\Delta u_n(t)$ and $\Delta u_n'(t)$ for typical fiber dispersion coefficients of $D = 17$ and 3.5 ps/km/nm. The initial launched pulse has an $1/e$ width of $T_0 = 5$ ps. Figure 7.7 shows that the nonlinear force of $\Delta u_n(t)$ due to the beating of $|u_0(z,t)|^2$ with $n(z,t)$ is far larger than the nonlinear force of $\Delta u_n'(t)$ due to the beating of $u^2(z,t)$ with $n^*(z,t)$. In term of power, the variance of $\sigma^2_{\Delta u_n'(t)}$ is less than 1% of $\sigma^2_{\Delta u_n(t)}$. The noise term of $\Delta u_n(t)$ also has more spreading over time than $\Delta u_n'(t)$. The spreading of $\Delta u_n(t)$ is more obvious for a high dispersion coefficient of $D = 17$ ps/km/nm. From Fig. 7.7, the contribution of $\Delta u_n'(t)$ to the nonlinear phase noise of the system can be ignored.

The temporal spreading of $\sigma_{\Delta u_n}(t)$ shows that ISPM phase noise spreads to adjacent symbols. Unlike Eq. (7.18) with an $1/e$ pulse width of about $\sqrt{3}T_0$, the profile of Fig. 7.7 has a pulse profile narrower than $\sqrt{3}T_0$ near the peak but a slow decreasing tail. For 40-Gb/s signal with $T = 25$ ps, the STD of $\sigma_{\Delta u_n}(t)$ at ± 25 ps is still very large, indicating that IXPM phase noise may be significant to the system with large

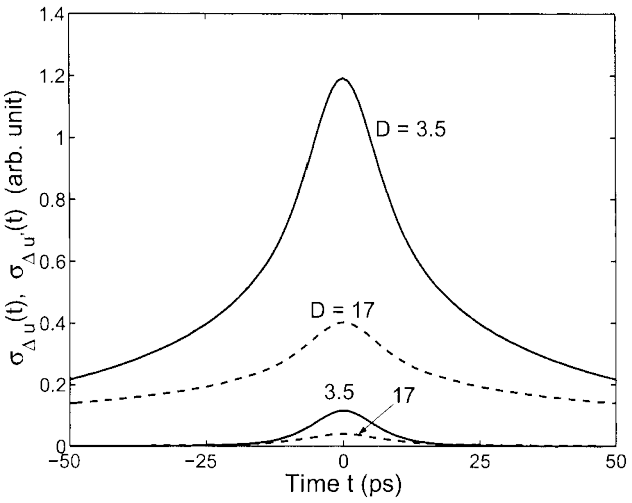

Figure 7.7. The temporal distribution of nonlinear force due to the beating of signal with noise. The upper two curves are $\sigma_{\Delta u_n}(t)$ and the lower two curves are $\sigma_{\Delta u'_n}(t)$.

pulse overlap. For the case with $D = 3.5$ ps/km/nm, $\sigma_{\Delta u_n}(t)$ at ± 25 ps is relatively smaller than that for the case with $D = 17$ ps/km/nm.

The temporal profile of Fig. 7.7 does not provide a direct answer to whether the spreading of $\sigma_{\Delta u_n}(t)$ can be ignored. Later part of this section will either include or exclude the IXPM phase noise. The temporal profile of Fig. 7.7 cannot be used directly to estimate the dependence between the nonlinear phase at $t = 0$ and, for example, $t = T$. As a trivial example for the signal of a system without chromatic dispersion and pulse distortion, the nonlinear force is always proportional to $|u_0(0,t)|^2 n(0,t)$. As white noise, the noises of $n(0,t)$ at $t = 0$ and $t = T$ are independent of each other. In this trivial case, the profile corresponding to Fig. 7.7 is proportional to $|u_0(0,t)|^2$.

If the nonlinear force of $\Delta u_n(t)$ is passing through an optical filter with an impulse response of $h_o(t)$, the filter output at the time of mT is

$$\begin{aligned}\zeta_{0,m} &= \int_{-\infty}^{+\infty} h_o(mT-t)\Delta u_n(t)\mathrm{d}t \\ &= 2j\gamma \int_{-\infty}^{+\infty}\int_{0}^{L} h_o(mT-t)\left\{\left[|u_0(z,t)|^2 n(z,t)\right]\otimes h_{-z}(t)\right\} e^{-\alpha z}\mathrm{d}z\mathrm{d}t.\end{aligned} \tag{7.40}$$

The ISPM phase noise from $\zeta_{0,0}$ is the noise generated by the beating of $|u_0(z,t)|^2$ with $n(z,t)$ and affects the DPSK pulse at $t = 0$. The IXPM

phase noise from $\zeta_{0,1}$ is from the beating of $|u_0(z,t)|^2$ with $n(z,t)$ and affect the DPSK pulse at $t = T$. Due to IXPM, the DPSK pulse at $t = 0$ also affects by the beating of $|u_1(z,t)|^2$ (the pulse at $t = T$) with $n(z,t)$ to give the IXPM phase noise of $\zeta_{1,0}$. Other than the temporal location, $\zeta_{1,0}$ is statistically the same as $\zeta_{0,-1}$. In general, $\zeta_{k,m}$ is statistically the same as $\zeta_{0,m-k}$. The term of $\zeta_{0,0}$ is ISPM phase noise and other terms of $\zeta_{l,m}$ with $l \neq m$ are IXPM phase noises.

For DPSK signal, the same as Fig. 7.3(b) to consider the differential phase, the differential nonlinear phase noise from both ISPM and IXPM phase noises is approximately equal to

$$\delta\phi_n = \frac{1}{A_0}\Im\left\{\sum_m \zeta_{m,0}\right\} - \frac{1}{A_1}\Im\left\{\sum_m \zeta_{m,1}\right\}. \tag{7.41}$$

For the optical pulses of $u_0(0,t)$ and $u_1(0,t)$, the optical filter of $h_o(t)$ is assumed to give an output of A_0 and A_1 at $t = 0$ and $t = T$, respectively. If the optical filter of $h_o(t)$ has a Gaussian impulse response and an $1/e$ pulse width of t_o, the impulse response is

$$h_o(t) = \frac{1}{\sqrt{2\pi}}\frac{\sqrt{t_o^2 + T_0^2}}{t_o T_0}\exp\left(-\frac{t^2}{2t_o^2}\right), \tag{7.42}$$

and

$$H_o(\omega) = \sqrt{1 + \frac{t_o^2}{T_0^2}}\exp\left(-\frac{1}{2}t_o^2\omega^2\right), \tag{7.43}$$

For simplicity, $A_0 = A_1$ is assumed for the same transmitted symbols in consecutive time intervals. As a circular complex random variables, the random variables of $\zeta_{0,m}$ has the property that $\Re\{\zeta_{0,m}\}$ and $\Im\{\zeta_{0,m}\}$ are independent and identically distributed. The variance of $\delta\phi_n$ is

$$\sigma^2_{\delta\phi_n} = \frac{1}{A_0^2}\left[\sum_{m_1}\sum_{m_2} E\left\{\zeta_{m_1,0}\zeta^*_{m_2,0}\right\} - \sum_{m_1}\sum_{m_2} E\left\{\zeta_{m_1,0}\zeta^*_{m_2,1}\right\}\right]. \tag{7.44}$$

Defined a function of $f_m(\omega)$ as

$$f_m(\omega) = 2\gamma|A_0|^2(T_0^2 + t_o^2)^{\frac{1}{2}}\int_0^L \frac{\exp\left\{-\frac{1}{2}t_o^2\omega^2 + \frac{\left[(t_o^2 - j\beta_2 z)\omega + jmT\right]^2}{\tau(z)^2 - 2j\beta_2 z + 2t_o^2}\right\}}{\sqrt{\tau(z)^2 - 2j\beta_2 z + 2t_o^2}} e^{-\alpha z}\mathrm{d}z, \tag{7.45}$$

where t_o is the $1/e$-width for the impulse response of $h_o(t)$, assumed that it is Gaussian pulse shape, we obtain

$$E\left\{\zeta_{m_1,0}\zeta^*_{m_2,0}\right\} = \frac{\sigma_n^2}{\pi}\int_{-\infty}^{+\infty} f_{m_1}(\omega)f^*_{m_2}(\omega)\mathrm{d}\omega \tag{7.46}$$